Information condensation in defect detection using TSR coefficients images

by J.-M. Roche*, F.-H. Leroy*, D.L. Balageas**

* ONERA, Composite Materials and Structures Dept., BP 72, 92322 Châtillon cedex
** Institute of Mechanics and Engineering of Bordeaux I2M, TREFLE Dept., 33305 Talence cedex, France

Abstract

The Thermographic Signal Reconstruction (TSR) technique, based on the logarithmic polynomial fitting of the temperature time-evolution, improves the efficiency of pulse-stimulated thermography. However, the non-destructive evaluation of the inspected structure requires the analysis of the full temperature-time sequence. This drawback impacts all transient thermal NDE method whatsoever. A new post-processing development of the TSR data, based on the use of the very limited number of polynomial coefficients, avoids this time-consuming task by producing a unique composite image of the defects, containing information on their depths. This image results from an RGB-basis projection of three of the most pertinent coefficient images.

The performance of the method is compared with that of the classic TSR method, in the case of a carbon/epoxy coupon containing artificial defects simulating delaminations. Comparisons are also made with three other well-known data processing techniques: Pulse Phase Thermography (PPT), Principal Component Thermography (PCT) and High-Order Statistics (HOS). In each case, the relevance of the new approach is proven: not only is it simple and rapid, but it also guarantees a defect detectivity at least as good as the one provided by the other techniques. Moreover, the RGB projection, successfully applied to all four methods (TSR, PPT, PCT and HOS), is shown to be an efficient operation to compress and synthesize the thermal data which was, so far, scattered in several images. It may be considered as a general post-processing technique useful for any such method currently used in NDE.

1. Introduction

If flash thermography is clearly the most sophisticated and versatile thermal non destructive evaluation (NDE) technique [1], this is certainly due to four decades of continuous research aiming at improving the detectivity and enhancing the accuracy of the characterization of defects [2]. The Thermographic Signal Reconstruction (TSR) technique [3-5] is the most recent improvement aiming at raising thermal NDE to the level of the most established NDE tools (ultrasonics, X-rays, liquid penetrant, magnetic particles and eddy currents). Although potentially allowing both qualitative and quantitative diagnoses, the technique is mainly remarkable for its performance in detection of defects, thanks to the use of logarithmic derivatives images which provide defect patterns of excellent quality. Nevertheless, the inspection of large sequences of thermographic images and experience in heat transfer are required to optimize the choice of the observation times for an optimal detection. To avoid these major drawbacks, data compression and data processing automation are essential. Studies have been carried out in this direction by using skewness and kurtosis [6,7].

In this article, a new TSR-based technique is proposed, to simplify the process of detecting defects and to obtain even better images. It is based on the use of the sole images of the coefficients of the logarithmic polynomials. The idea to considerer the TSR coefficients images is not totally new: it was tested by Vavilov [8] and Grinzato [9], while the TSR technique was spreading in the NDE community. A brief comparison of this type of images to Principal Component Thermography (PCT) and phasegrams from Pulse Phase Thermography (PPT) was also made by Umar et al. [10]. More recently, a study was carried out by Dumoulin et al. [11], using logarithmic polynomials to produce images of defects embedded in asphalt pavement samples submitted to a long square-shaped heat flux.

Once the principle of the TSR processing technique is recalled (Section 2), the new approach is introduced (Section 3) and applied to the inspection of a carbon/epoxy coupon (Section 4). The optimization of the degree of the fitting polynomial is carefully examined and a strategy to produce a unique composite color image is proposed and implemented. The obtained results are then compared with the ones of the classic TSR technique (Section 5), and the ones from PCT, PPT and High-Order Statistics (HOS) techniques (Section 6).

2. Classic TSR technique

The TSR method applied to pulsed thermographic experiments, for NDE purposes, consists in:
- the fitting of the experimental log-log plot thermogram (here, the word "thermogram" will refer to a "pixel temperature time-history", although in literature it can refer to a "thermal image") by a logarithmic polynomial of degree n:

$$\ln(\Delta T) = a_0 + a_1 \ln(t) + a_2 \left[\ln(t)\right]^2 + \ldots + a_n \left[\ln(t)\right]^n \tag{1}$$

with ΔT the temperature increase as a function of time t (thermogram) for each pixel (i,j). This fitting is very useful for data storage since it enables to replace the full sequence of temperature rise images, ΔT(i,j,t) by the series of (n+1) images of the polynomial coefficients: a_0(i,j), … a_n(i,j) (Figure 1). From this series of (n+1) images, it is possible to rebuild a full thermographic sequence.

- the computation of the 1st and 2nd logarithmic derivatives of the thermograms, the derivation being achieved directly on the polynomial, therefore with a limited increase of the temporal noise.
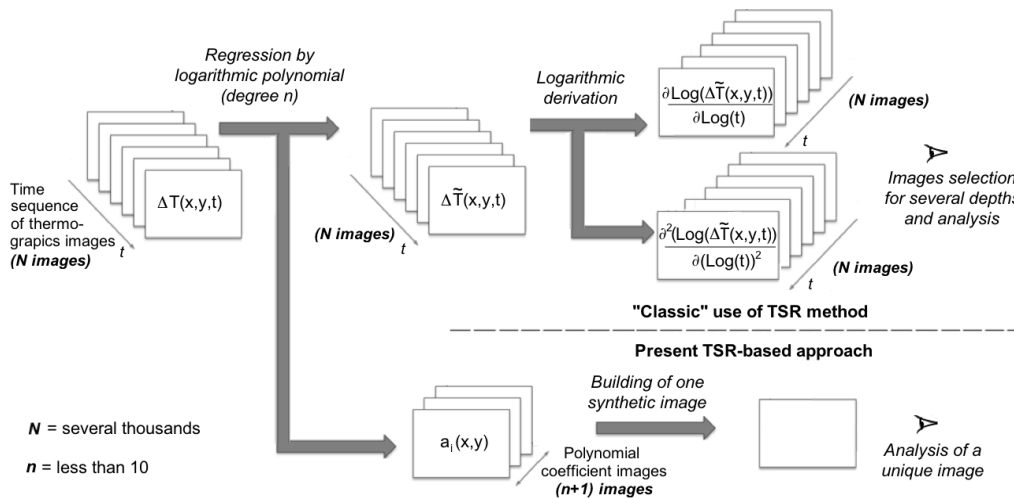

Fig 1. Defect detection by the TSR method: "classic" use and present approach.

The sequences of images of the derivatives can be either qualitatively observed to detect the defects (Fig. 1), or quantitatively used to evaluate the depth of a defect, from characteristic times such as the half-rise time of the first derivative or the time of the maximum of the second derivative. This quantitative data analysis is out of the scope of the present work.

3. A simple TSR-based technique for a rapid and efficient detection of defects

The application of the TSR post-processing technique, as it is described in the previous section, requires the calculation of (*n*+1) logarithmic polynomial coefficients for every pixel, which implies the generation of (*n*+1) images giving the distribution of these coefficients. So far, these images have been almost exclusively considered as an intermediate step in the TSR process, and not fully exploited for direct detection of defects.

However, such images contain information on the internal structure, which might be sufficient to detect all embedded defects. This would be very convenient, since it would drastically reduce the data amount to consider, from the full sequence of temperature rise images ΔT (i,j,t) to a small series of (*n*+1) images of polynomial coefficients a_0(i,j), a_1(i,j), …, a_n(i,j). The calculation of the images of logarithmic derivative distributions and the time-consuming process of selection of the most adequate images (one for each depth) could be avoided, as long as the purpose is pure detection, to a qualitative level only.

In the following sections, the interest of this new approach is illustrated for the detection of artificial defects of various sizes and depths, in a carbon/epoxy composite plate. An empirical description of the polynomial coefficients images is done and an optimization of the method for a practical use is made. Answers are brought to questions which immediately arise: how the information on defects is distributed among the various coefficient images? What is the optimal polynomial degree to obtain the better defect images? Is it possible to compress all information in a unique composite image? Are these images of better quality than those resulting from the distributions of the first and second derivatives? How can they be compared to other known techniques such as PCT, PPT and HOS?

4. Application to a structure with defects of well defined location depths

The tested coupon is a 270 mm × 200 mm × 5.25 mm carbon/epoxy composite plate, which has already been used for various studies in the past [12,13]. Its thermal diffusivity was preliminary measured by a classic flash diffusivity experiment and found equal to $(4.2 \pm 0.2)\ 10^{-7}$ m^{2}s^{-1}. The coupon contains 80 μm-thick Teflon® inserts of various sizes, embedded at different depths during the fabrication process of the composite, so that the influence of the defect depth and size can be analyzed. Furthermore, two zones contain two stacked up inserts of different sizes at different depths. The characteristics of the defects (shapes, dimensions, depth locations) are given in Fig. 2. They result from information given by the constructor and from ultrasonic measurements. The coupon is coated by a black, thin, carbon layer on both faces. The defects are numbered by two figures, the first one indicating their sizes, the second one their depths.

The tests were carried out at the Composite Materials and Structures Dept. of ONERA, using two Elinchrom flash lamps delivering a pulse of total energy 6 kJ in 4 ms. The temperature images (320 x 256 pixels) were recorded during 60 s at 200 Hz, with an integration time of 230 μs, by a CEDIP Jade LWIR camera. A Plexiglas® filter was put between the sources and the coupon to mitigate the spurious infrared radiations emitted by the hot flash lamps after the pulse. The inevitable non-uniformity of the heat deposition on the coupon was corrected by normalization.
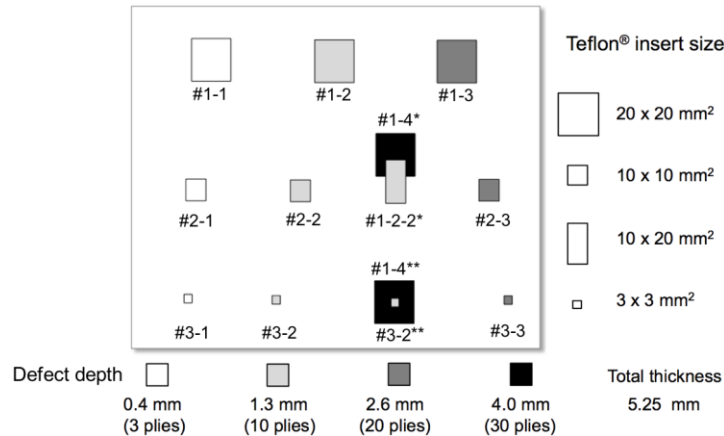

Fig. 2. Tested carbon/epoxy coupon: distribution of the artificial defects established from constructor information and ultrasonic measurements.

Fig. 3 presents the time evolution of the surface temperature increase of the coupon after the pulse deposition (*t*=0) in the center of defect #1-1 and that of the sound zone (mean of eight points). The temperature increases have been normalized by those of an early time for which thermograms are not influenced by the shallowest defects. The slope of the sound zone thermogram is very close to -1/2. The noise of the thermograms becomes important after 20 s, and for deeper defects, not presented in this figure for sake of readability, the contrast between defective and sound zones might be merged in the noise, making the fitting by logarithmic polynomials a necessity.
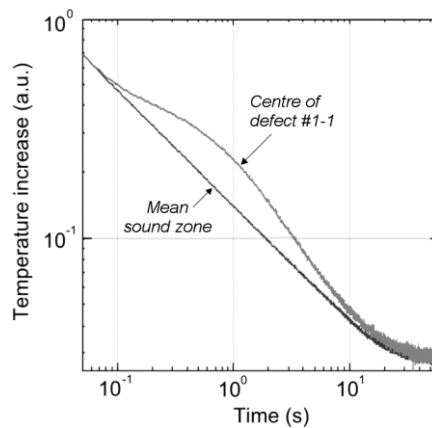

Fig. 3. Time evolutions of normalized temperature increases for sound zone and defect #1-1, after the 4 ms pulse.

4.1. Constitution of the coefficient images

The coefficient images are presented with a grey scale obtained by giving the black colour to the pixels having the lowest coefficient algebraic value and the white colour to the pixels having the highest coefficient algebraic value. The sound regions have a grey level resulting from the linear interpolation between minimum and maximum coefficient values. To avoid any distortion of this scale, a post-processing routine replaces the dead or abnormal isolated pixels by the median of their neighbors.

4.2. Choice of an optimal polynomial degree

To be relevant, the method must lead to images containing the highest possible number of defects present in the coupon. The optimization of the method requires a fine understanding of the combined influence of the two following parameters: the polynomial degree and the coefficient rank. Therefore, it is necessary to make a detailed analysis of the coefficient images generated by the logarithmic polynomial fitting.

For the present experiment, the fitting by logarithmic polynomials has been done for degrees n varying from 3 to 11. For each degree, the images corresponding to the coefficients of ranks 0 to n are given in Fig. 4. Each coefficient image is identified by a label, the sign of which being negative if the grey scale is inverted, to make the images more comparable to each other, constituted of two numbers corresponding to the coefficient rank and the polynomial degree. For instance, the image labelled "–4/8" is the (x,y)-distribution of the coefficient a4 of the polynomial of degree 8, represented with an inverted grey scale; the label "5/8" corresponds to the coefficient a5 of the same polynomial, with the normal grey scale.
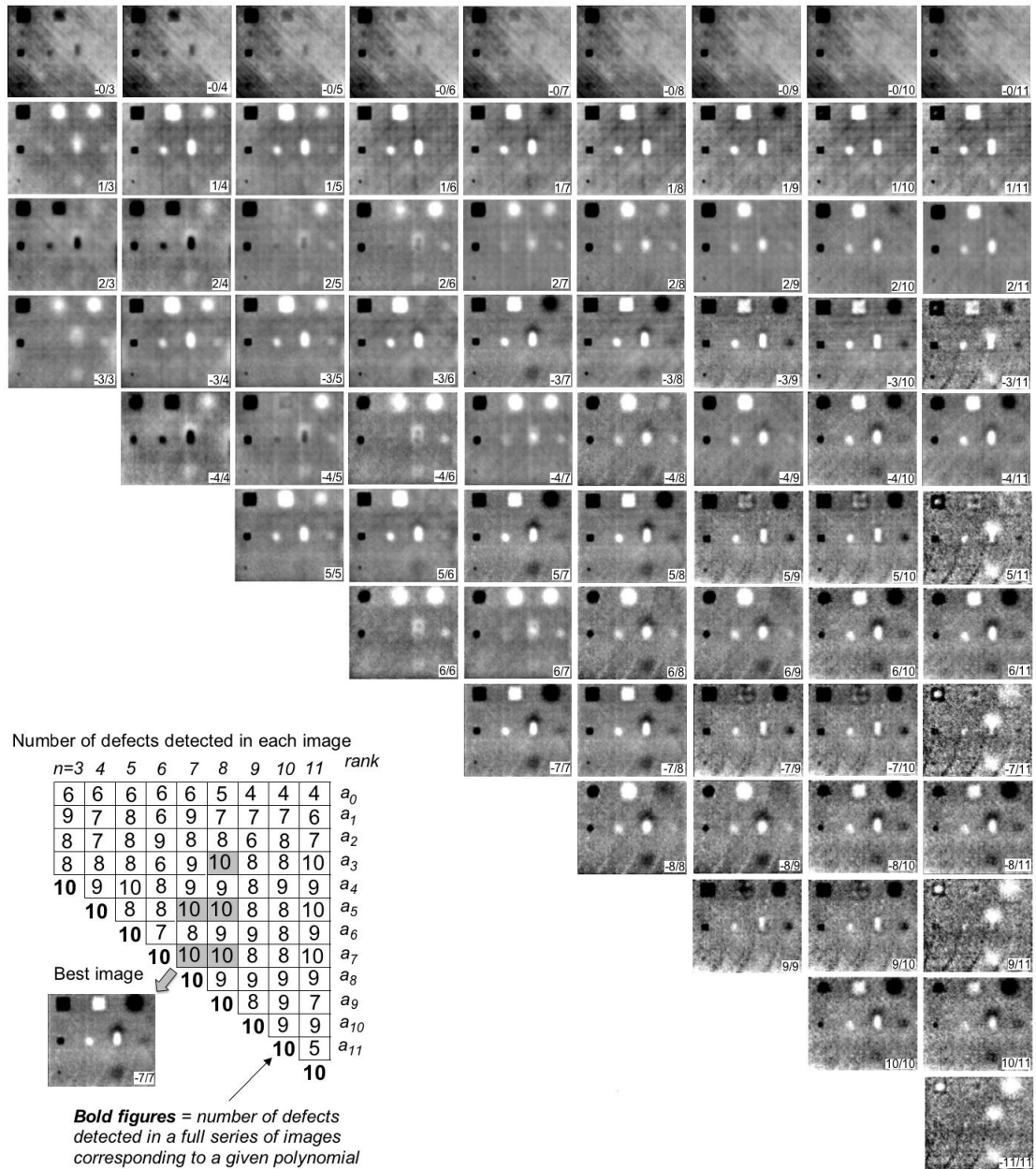

Fig. 4. *Pulse-heating coefficient images for polynomial degrees from 3 to 11. Influence of the polynomial degree and of the coefficient rank. Selection of an optimal polynomial degree (here n=7).*

A few general qualitative trends can be drawn from the comparisons of the images presented in Fig. 4:

i) To make the images more similar, for any polynomial degree, it is necessary to invert the grey scale one time over two, separately considering the odd and even ranks, and attributing opposite signs to the first two ranks (0 and 1). This ultimately leads to the following series of images: -0/n, 1/n, 2/n, -3/n, -4/n, 5/n, and so on.

ii) Odd rank images are always sharper than even rank images, whatever the polynomial degree, and most of the time, more defects can be detected in the odd rank coefficient images than in the previous and following even rank coef-

ficient images. This might be due to the odd symmetry of the logarithmic thermograms of the defective zones. Nevertheless, more experience is needed to determine whether this trend is caused by the present type of defects or is more general.

iii) A constant influence of the defect depth on the image sharpness is noted: the deeper the defect, the less sharp the image. The shape of the deepest defects may even become evanescent.

iv) The sign of the contrast generated by the defect may change, possibly several times, with increasing depths.

v) Defects located at the same depth always present the same grey level, at least for degrees inferior to 9. For polynomial degrees higher than 8, the texture of extended defects may become complex.

vi) The number of detected defects tends to increase with the coefficient rank. However, this trend is a bit erratic.

vii) The noise increases with the polynomial degree.

viii) The first two coefficient images (a_0 and a_1) reveal the first two surface plies (-45° and +45°); for higher ranks, the other plies (90° and 0°) are also visible, but mixed, and with an increasing noise. These images can be used just like tomographic cross-sections, with a space resolution which, obviously, decreases with the investigated depths.

In order to select the optimal degree, as for defect detections, the number of visible defects in each image has been evaluated by visual examination. Defects #3-2, 3-2** and 3-3 can be considered as non-detectable in the present experimental conditions, because of the combined 3D conduction effects (side over depth ratios between 2.3 and 1.15), their near-resolution characteristic size (side inferior to 4 pixels), and their limited equivalent finite resistances. The maximum number of detectable defects can then be set equal to 10 (defects #1-1, 2-1, 3-1, 1-2, 2-2, 1/2-2*, 1-3, 2-3, 1-4*, and 1-4**), so that the quality of the images and the efficiency of the method are evaluated by comparing the number of defects detected with the naked-eye to 10. The results are displayed in Figure 4: the bold figure at the bottom of each column represents the number of detected defects considering the full series of coefficient images for a given polynomial. It appears that for all explored values of n, all detectable defects are visible in such a series of images.

The second evaluation indicator for this method is to find a coefficient image containing all detectable defects, for the lowest polynomial degree. Image -4/5 could be selected, but defects #1-2, 2-3 and 1-4** are hardly visible, so that it seems more sensible to pick degree 7 or 8. For these two degrees, there are respectively two and three images revealing the full collection of detectable defects. Among these five complete images, image -7/7 can be considered as the best quality image. Complete defect images are also found for $n = 10$ and 11, but are definitely noisier.

Based on these considerations, degree 7 can be selected as the optimal degree for defect detection in this tested coupon.

4.3. Production of a unique synthetic image of the defects

To make our approach even more convenient and efficient, the final step would be to set an automatic procedure producing *one* synthetic image (from the series of coefficient images), in which all detectable defects would be visible. The ultimate level of data compression would be reached, since no user intervention in the image selection process would be needed.

At this point, it is worth noticing that the five complete images (5/7, -7/7, -3/8, 5/8 and -7/8) are all odd rank images. It can be inferred that the sole odd images can be used to build the wanted synthetic image. The other advantage of not choosing the even images is an increase of the sharpness of the final image. In this case, considering degree $n = 7$, the summing of images 1/7, -3/7, 5/7 and -7/7 gives a satisfactory result, but defect #2-3 is hardly visible in the synthetic image (Fig. 5a). To have a proper detection of this defect, the summing of even images (-0/7, 2/7, -4/7, 6/7) is much better, but defect #1-4** is totally missing (Fig. 5b). Since the final result is not as convincing as expected, another procedure should be set up.
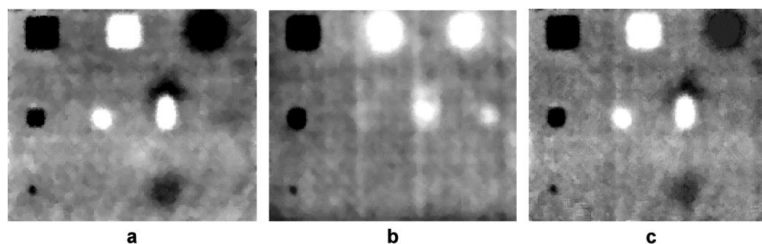

a   b   c

Fig. 5. (**a**) *Synthetic image of the defects obtained by summing all odd coefficients of the polynomial of degree 7 (images 1/7, -3/7, 5/7,-7/7);* (**b**) *ditto considering the even coefficients (images -0/7, 2/7, -4/7, 6/7);* (**c**) *ditto considering the three highest rank coefficient images (images 5/7, 6/7,-7/7).*

It is also noticeable that all detectable defects can be seen when considering the three highest order images, no matter the polynomial degree. In particular, for degree 7, all ten defects are neatly detected in the trio (5/7, 6/7, -7/7). Nevertheless, summing the three images leads to an unsatisfying result (Fig. 5c) because defect #2-3 generates contrasts with opposite signs in odd and even images. Therefore, the solution proposed in this article consists in projecting these three images in an RGB basis. The resulting composite image, displayed in Fig. 6a, makes all ten defects appear, with no possible doubt for an operator, which was the whole point of the present study.
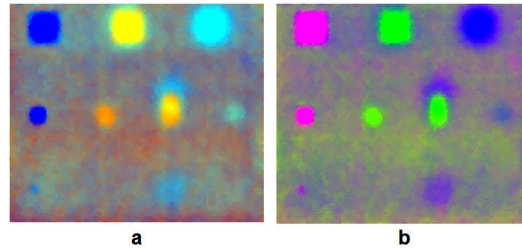
Fig. 6. *Synthetic composite image obtained by the projection of a trio of coefficient images in an RGB basis and influence of the choice of the coefficient images on the color of the defects: (a) trio: 5/7, 6/7,-7/7;(b) trio: -4/7, 6/7,-7/7. Caution: if reproduced in grey tones, this color image will not be meaningful.*

Assuming that all the defects have the same severity, which is realistic here since they are artificial and identically made, it can be noted that a bi-univocal relation exists between color and defect depth. Moreover, for one given depth, various shades are observed: for instance, defect #1-2 appears in bright yellow, while defect #2-2, for which 3D conduction effects are not negligible given its small dimensions, appears in orange; as for defect #1/2-2*, a gradient of color from the top to the bottom is seen, due to the influence of defect #1-4* which is partially underneath it. This is definitely an additional valuable piece of information given by the composite image, even though the color scale has no absolute value. The color range indeed depends on the images chosen the build the composite one, as it is checked in Fig. 6b, which displays a similar RGB projection, for the {-4/7, 5/7, -7/7} trio.

This depth/color dependency should be studied more thoroughly, since it could give even more credit to the present technique. However, experimental data with real defects (such as delaminations) is needed: this will be the object of future works already initiated in ONERA.

5. Comparison of the present method to the classic TSR method

5.1. Optimization of the polynomial degree and estimate of the logarithmic derivatives

The choice of the optimal polynomial degree in the previous section was exclusively based on the coefficient images quality. The classic TSR technique is centered on the analysis of the first and second logarithmic derivatives of the thermograms. For this purpose, it is necessary to obtain the most precise fitting of the thermograms. Therefore, the choice of the optimal polynomial might not be the same: in the present case, it has indeed been found that the optimum fit was obtained for a higher polynomial degree: n=11, a degree which is higher than what is usually found in literature.

These results on optimal degrees (7 or 8 for defect imaging and detection; 11 for time analysis of logarithmic derivatives) are coherent with the numerical simulations and experiments mentioned in [11] where the TSR technique is applied to squared-shaped heating thermographic tests, exploiting the relaxation phase of the thermograms. The degree 5 is used to produce TSR coefficient images and degrees 9 and 10 for pulse-phase analysis. When using the whole square heating sequence, the best fit required to reach degrees as high as 13 or 14.

5.2. Optimization of the observation time for defect detection in the derivative images

The optimization of the defect detection using the logarithmic derivatives consists in selecting the observation times which give the best SNR and sharpness compromise. This requires an analysis of the full sequences of the derivative images (see Fig. 1). Fig. 7 illustrates this issue by presenting the time evolution of the first and second logarithmic derivatives at the center of the largest defects located at the four depth levels and in the sound area. The choice of the optimal observation times for each depth is made by looking for the maximal contrasts between the defective zone curves and the sound zone ones.
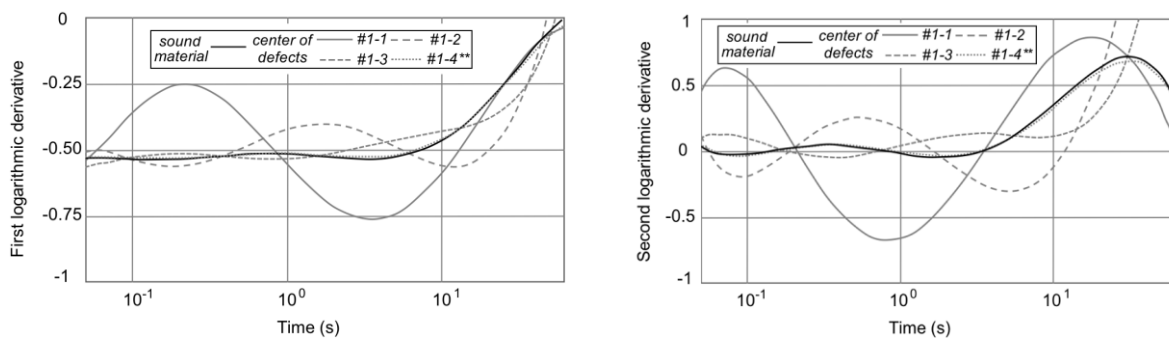

Fig. 7. *Logarithmic derivatives of the sound zone (mean over 8 locations) and at the centers of the defects of maximum size (20x20 mm): first (on the left) and second derivative (on the right). Polynomial of degree: 11.*
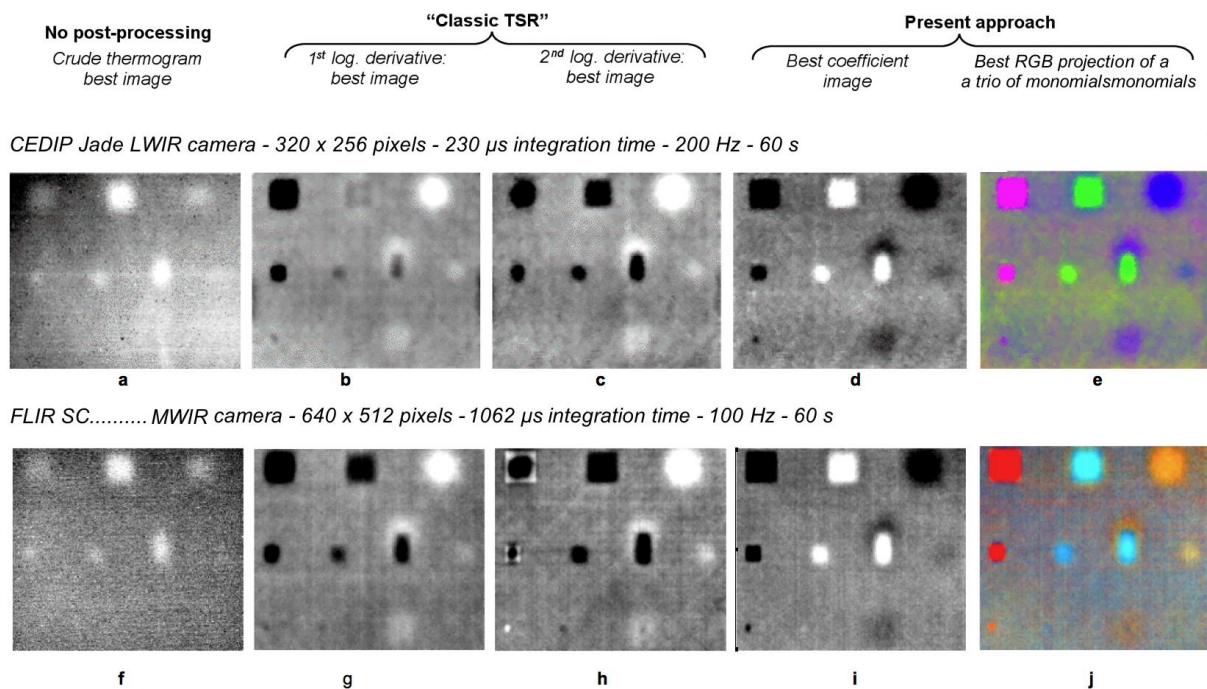
No post-processing	"Classic TSR"		Present approach	
Crude thermogram best image	*1st log. derivative: best image*	*2nd log. derivative: best image*	*Best coefficient image*	*Best RGB projection of a a trio of monomialsmonomials*

CEDIP Jade LWIR camera - 320 x 256 pixels - 230 µs integration time - 200 Hz - 60 s

a   b   c   d   e

FLIR SC.......... MWIR camera - 640 x 512 pixels - 1062 µs integration time - 100 Hz - 60 s

f   g   h   i   j

Fig. 8. *"Best" images obtained by the application of the TSR and TSR-based techniques. Influence of the IR camera.*
***First row**: Present experiment with a Cedip Jade camera. (**a**) best thermal image at time 7.5 s; (**b**). Classic TSR method: First logarithmic derivative (polynomial of degree 11) at time 3.5 s; (**c**) ditto, second logarithmic derivative (polynomial of degree 11) at time 2.3 s; (**d**) Present TSR-based method: best coefficient image (polynomial of degree 7, image coefficient of rank 7); (**e**) RGB projections of the monomials 5/7, 6/7 and -7/7.*
***Second row**: Present experiment with a FLIR X6540sc camera (images taken from [20]). (**f**) Thermal image at 10 s; (**g**) First logarithmic derivative (polynomial of degree 7) at time7.5 s; (**h**) ditto, second logarithmic derivative at time 2.5 s; (**i**) Present TSR-based method: best coefficient image (polynomial of degree 7, image coefficient of rank 5); (**j**) RGB projections of the monomials 2/7, -3/7, and 5/7.*

The images providing a maximum number of visible defects, are obtained at time 3.5 s for the first logarithmic derivative (Fig. 8b) and at time 2.3 s for the second logarithmic derivative (Fig. 8c). They are compared to the best crude image (Fig. 8a), which is given as a reference and a demonstration of the necessity of data processing for thermographic NDE applications, and to the best coefficient image (Fig. 8d), that is to say the -7/7 one, chosen as explained in the previous sections. Finally, the composite image presented in Figure 6 is given for comparison in Figure 8e. But even without this composite image, the best image, based on defect detectability, is still given by the present approach.

6. Influence of the camera performance

The camera used for the aforementioned experiments was a ten-year-old CEDIP Jade LWIR camera (320 x 256 pixels) with a non-negligible number of defective pixels (dead or erratic). In order to study the sensitivity of the present method to the noise of the recorded images, the present experiment results are compared to the ones obtained with a more recent camera, the FLIR X6540sc camera (640 x 512 pixels) [20]. The matching images are given in Figure 8 (f-j).

The new set of images presents some advantages, in particular:
i) the background (non defective areas) is more uniform (which may be attributed to a less noisy normalisation operation thanks to the camera performance);
ii) thanks to the higher number of pixels of the recent camera, the space resolution is better, which gives more contrasted defect contours and enables to detect more defects, in particular defects #3-2 and #3-2** which are not seen in the first set of images (first line).
Considering the number of clearly detected defects, the image 8h is certainly the best one, nevertheless, the pattern of the defect images becomes complex for the shallowest defects, which may make the detection of irregularly-shaped defects and of superposed defects more difficult.

It can be concluded that there is a slight influence of the noise of the cameras on the quality of the images and that the higher number of pixels of the second camera definitely improves the space resolution of all processed images, allowing to detect the less extended defects.

7. Comparison to other data processing techniques

The exact same experimental data have been processed using well-known methods currently used in thermographic NDE: PCT [14,15], PPT [16,17], and HOS [7].

The first set of approaches (PPT, PCT) proposes alternate bases for projection. While the TSR method projects onto a logarithmic polynomial basis, PPT relies on the Fourier basis (discrete Fourier transform) – so, the PPT technique used here is a significant extension of the well-known technique in which phase images are calculated for various frequencies in relation with the supposed defect depths –, and PCT defines an optimal empirical projection basis obtained by analysis of the signals (Singular Value Decomposition). For PPT the most valuable information is contained within the five phase images related to the lower frequencies. Similarly, for PCT the first five components related to lower eigenvalues are potentially meaningful. It is worth mentioning that, as underlined by Marinetti *et al.* [15], PCT can be performed on frames (space components) or thermograms (time components); in our case, results turned out to be slightly better with time components. The HOS approach is also based on the analysis of time profiles but no projection basis is required. Profiles are analyzed through their statistical behaviour. Each thermogram is characterized by the central moments of the distribution of recorded temperatures. Subsurface defects are potentially detected by contrasts in moments up to order 5. The mean, variance, skewness and kurtosis correspond to the first, second, third and fourth moments, respectively.

The same approach (RGB projection of the three selected images) is applied to the three methods (PCT, PPT and HOS), and compared to the results obtained with the present TSR-based approach (Fig. 9). The first observation that can be made is that the procedure is not very conclusive for the HOS technique: the mean grey levels of the three images (skewness, kurtosis and 5th order) are so close to each other that the resulting image remains in grey tones too. As for the PCT and PPT techniques, the composite RGB images give satisfactory results, but the TSR composite image is still the best: more detected defects, higher color contrast, better sensitivity of the colors to the defect depths and lower noise in the sound zone (disappearance of the patterns due to the structure of the composite, constituted of plies of various orientations).
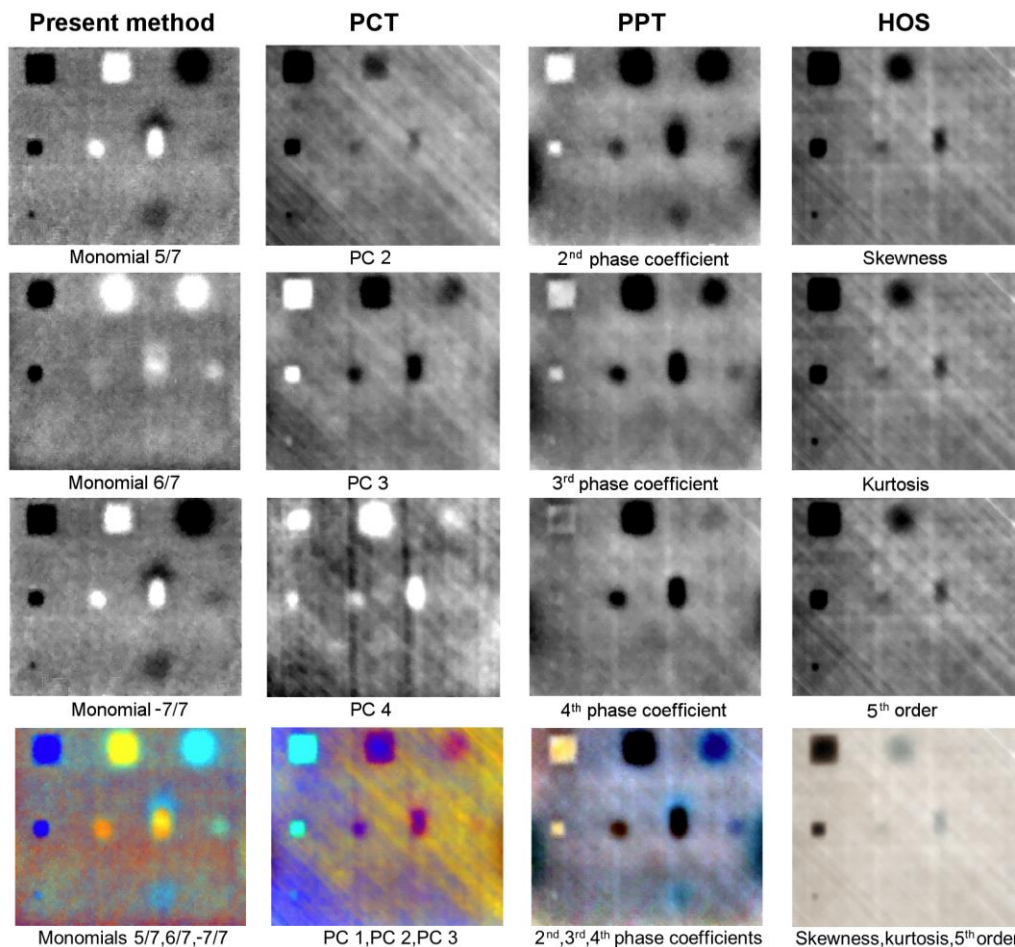

Fig. 9. *Comparison of the present TSR-based method to other data processing techniques producing defect images. First three top lines: grey level images (256 bits) of individual component; bottom line : RGB projection of these components.* Caution: if reproduced in grey tones, the colour images of the bottom line color will not be meaningful.

From a computational point of view, the present approach is comparable to PPT and HOS: they are all very fast. The different processing operations were performed with MATLAB on a 2 Quad-Core Intel Xeon 2.53 GHz Windows PC with 12 GB RAM. For the 12,000 frames sequence considered here (processed zone of 194x166 pixels), extraction of coefficient images takes 14 s, to be compared to 19 s for PPT or HOS. On the contrary, the PCT approach is very demanding in memory (12 GB required) and time consuming (half an hour) though a computational strategy for the SVD was used to take into account that frames are less numerous than pixels in our example [15].

Although these comparisons remain mostly qualitative, it can be concluded that the present method gives excellent results, both in terms of defect detectivity and in terms of processing rapidity. A more quantitative comparison of the images of Fig. 9 will be performed in the near future, based on the evaluation of the signal-to-noise ratio (SNR) and of the sharpness of every defect, for all images and all methods.

8. Conclusions

The point of the present work was to propose a post-processing technique aiming at improving the detection of defects in structures using pulsed thermography. One major stake was that the technique had to be usable by operators, typically in an industrial context, with no necessity for them to have any experience in the heat transfer science field. Therefore, not only the whole procedure had to be fully-automated, with a restitution time as short as possible, but also the final result had to enable a reliable detection of defects, with minimal subjectivity. The approach suggested in this article is to take full advantage of the coefficients of the logarithmic polynomials used by the TSR technique, which were unexploited for themselves so far, by producing a unique composite image resulting from the projection of the three highest-rank coefficient images in an RGB basis. It is applied to a pulse thermography experiment carried out on a carbon/epoxy coupon, containing artificial defects embedded at various depths (up to 4 mm). The results highlight the numerous advantages of this new TSR-based technique:

- as long as detection only is aimed at, all defect information is contained in this one composite image, so that no time-consuming image selection process is needed anymore;
- the construction of the composite image does not need to define a sound zone, which is usually a burning issue in NDE by pulse thermography;
- even though the composite image cannot be used *a priori* to identify the depths of the detected defects, each color level is associated with a given depth, assuming that their severity is identical from one another.

The logarithmic polynomial fitting is now considered as a basic pre-processing operation, useful for any data processing adapted to pulse thermography [18,19], the present method included. Once the logarithmic polynomial fitting achieved, the extra-time required to build the RGB composite image is almost negligible: less than one minute on a regular laptop computer for the present experiment, during which 12,000 thermographic images of 320x256 pixels were recorded and processed. The objective in terms of time processing reduction is then reached too.

The qualitative comparisons that were made with other well-known data processing techniques, such as PCT, PPT and HOS, confirm the value of the present method, both in terms of efficiency to detect defects and in terms of simplicity and rapidity. Obviously, the procedure now needs to be applied to other types of materials and structures. Several studies are already in progress in ONERA, among which the detection of manufacturing defects in new-generation woven composite materials.

Furthermore, the presently proposed RGB projection was successfully applied to the three other tested methods (PCT, PPT and HOS) and was found efficient to compress and synthesize the thermal data which was, so far, scattered in several images. In the near future, and for the particular case of the TSR method, the RGB projection will be improved following three directions:

- automation of the selection of the three components to be projected;
- optimization of the final composite image in order to maximize the defect detectability by taking into account the human eye sensitivity to each of the RGB colors (what color should be attributed to each component, with what amplification);
- assessment of the defect depth information contained in the composite image.

Acknowledgements

9. References

[1] Spring, R., R. H. Huff and M. Schwoegler, "Infrared thermography: a versatile nondestructive testing technique", *Materials Evaluation*, Vol. 69, No. 8, pp. 934-942, 2011.
[2] Balageas, D. L., "Defense and illustration of time-resolved thermography for NDE", *Quantitative InfraRed Thermography Journal*, Vol. 9, No. 1, pp. 5-38, 2012.

[3] Shepard, S.M., "Advances in pulse thermography", *Thermosense XXIII Proc.* Vol. 4360, pp. 511-515, 2001.

[4] Shepard, S. M., J. R. Lhota, B. A. Rubadeux, D. Wang D. and T. Ahmed, "Reconstruction and enhancement of active thermographic image sequences", *Optical Engineering*, Vol. 42, No. 5, pp. 1337-1342, 2003.

[5] Shepard, M., "Thermography of composites", *Materials Evaluation*, Vol. 65, No. 7, pp. 690-696, 2007.

[6] Albendea P., Madruga F.J., Cobo A., López-Higuera J.M., "Signal to noise ratio (SNR) comparison for pulse thermographic data processing methods applied to welding defect detection", *Proc. 10th QIRT Conf.,* 2010. QIRT Open Archives: http://www.qirt.org/dynamique/index.php?idD=50, paper # QIRT 2010-004.

[7] Madruga F.J., Ibarra-Castanedo C., Conde O.M., López-Higuera J.M., Maldague X., "Infrared thermography processing based on higher-order statistics", *NDT&E International*, Vol. 43, pp. 661-666, 2010.

[8] Vavilov V. "ThermoFit Pro operation manual", Russia, Innovation Ltd., 82 p., 2000.

[9] Grinzato E., "Temperature monitors works of art health as human beings", 16th World Conference on Non destructive Testing, 30 August – 3 September 2004, Montreal (Canada). Available at: http://www.ndt.net.

[10] Umar M.Z., Ahmad I., Vavilov V., Swiderski W., Hamzah A.R., Wan Abdullah W.S.," Developing methodology of pulsed thermal NDT of materials: step-by-step analysis of reference samples", *NDT.net.* : http://www.ndt.net.

[11] Dumoulin J., Ibos L., Marchetti M., Mazioud A., "Detection of non emergent defects in asphalt pavement samples by long pulse and phase infrared thermography", *European Journal of Environmental and Civil Engineering*, Vol. 15, pp. 557-574, 2011.

[12] Balageas D. L., Déom A. A., Boscher D. M., "Characterization and non destructive testing of carbon-epoxy composites by a pulsed photothermal method", *Materials Evaluation,* Vol. 45, No. 4, pp. 461-465, 1987.

[13] Krapez J.-C., D. Boscher, Ph. Delpech, A. Déom, G. Gardette, D. Balageas, "Time-resolved pulsed stimulated infrared thermography applied to carbon-epoxy non destructive evaluation", *Proc. 1st QIRT Conf. 1992.* QIRT Open Archives: http://qirt.gel.ulaval.ca/dynamique/index.php?idD=55, paper # QIRT 1992-029.

[14] Rajic N., "Principal component thermography for flaw contrast enhancement and flaw depth characterisation in composite structures," *Composite Structures*, Vol. 58, No. 4, pp. 521-528, 2002.

[15] Marinetti, S., E. Grinzato, P. G. Bison, E. Bozzi, M. Chimenti, G. Pieri and O. Salvetti, "Statistical analysis of IR thermographic sequences by PCA", *Infrared Physics & Technology*, Vol. 46, No. 1–2, pp. 85-91, 2004.

[16] Maldague X., Marinetti S., "Pulse phase infrared thermography", *J. Appl. Phys.,* Vol. 79, pp. 2694-2698, 1996.

[17] Ibarra-Castanedo C., Maldague X., "Pulsed phase thermography reviewed", *Quantitative InfraRed Thermography Journal,* Vol. 1, No. 1, pp. 47-70, 2004.

[18] Klein M., Bendada A., Ibarra-Castanedo C., Maldague XPV. "A hybrid pulsed thermography processing technique for depth estimation of subsurface defects combining TSR and PPT". *Proc. 10th QIRT Conf.* 2010. QIRT Open Archives: http://www.qirt.org/dynamique/index.php?idD=50, paper # QIRT 2010-066.

[19] Usamentiaga R, Venegas P,Guerediaga J, Vega L, López. "A quantitative comparison of stimulation and post-processing thermographic inspection methods applied to aeronautical carbon-fibre reinforced polymer". *Quantitative InfraRed Thermography Journal,* Vol. 10, No 1, pp. 57-75, 2013.

[20] Roche J-M, Balageas DL."Common tools for quantitative pulse and step-heating thermography – part II: experimental validation". QIRT 2014 Conf. Bordeaux, 7-11 July 2014.